[redacted]

NASA TECHNICAL MEMORANDUM

UB
NASA TM X-1189

UB
NASA TM X-1189

ATLAS-CENTAUR FLIGHT AC-4 COAST-PHASE PROPELLANT AND VEHICLE BEHAVIOR

by Steven V. Szabo, Jr., William A. Groesbeck, Kenneth W. Baud, Andrew J. Stofan, Theodore W. Porada, and Frederick C. Yeh

Lewis Research Center
Cleveland, Ohio

NATIONAL AERONAUTICS AND SPACE ADMINISTRATION • WASHINGTON, D. C. • DECEMBER 1965

[redacted]

[redacted]

NASA TM X-1189

ATLAS-CENTAUR FLIGHT AC-4 COAST-PHASE PROPELLANT AND VEHICLE BEHAVIOR

By Steven V. Szabo, Jr., William A. Groesbeck, Kenneth W. Baud, Andrew J. Stofan, Theodore W. Porada, and Frederick C. Yeh

Lewis Research Center
Cleveland, Ohio

NATIONAL AERONAUTICS AND SPACE ADMINISTRATION

[redacted]

[redacted]

ATLAS-CENTAUR FLIGHT AC-4 COAST-PHASE PROPELLANT AND VEHICLE BEHAVIOR

by Steven V. Szabo, Jr., William A. Groesbeck, Kenneth W. Baud,
Andrew J. Stofan, Theodore W. Porada, and Frederick C. Yeh

Lewis Research Center

SUMMARY

The Atlas-Centaur flight AC-4 was the fourth in a series of research and development flights. The flight sequence included a 25-minute coast after injection into a 90 nautical-mile circular orbit. A coast-phase experiment was planned to evaluate controlled venting of the hydrogen tank, a second engine start at the end of the coast period, and a turnaround and retromaneuver to simulate separation from the spacecraft.

Parts of the coast-phase experiment were not accomplished primarily because of an uncontrolled propellant behavior excited by vehicle disturbances at the first Centaur main engine cutoff. The combined effects of engine shutdown transients, vehicle dynamics, and other energy inputs to the propellants, induced a forward displacement and circulation of the liquid residuals within the tank. Viscous damping of the liquid hydrogen was insufficient to dissipate the propellant kinetic energy, and the propellant settling motor thrust, producing an artificial gravity level of about 3×10^{-4} g, was inadequate to prevent liquid motion (due to kinetic energy) from covering the vent opening at the "forward" end of the hydrogen tank. Failure to settle the liquid hydrogen at the time of venting resulted in venting of mixed-phase or liquid flow, which, on expanding from the vent exits, produced high impingement forces in excess of the attitude control system capability, and the vehicle tumbled out of control. Continued tumbling centrifuged the liquid hydrogen to the forward end of the tank. Subsequent venting of the liquid hydrogen to maintain tank pressures depleted the residual and prevented accomplishment of the remaining coast-phase experiments.

INTRODUCTION

The advent of cryogenic propellants for upper stage space vehicles with missions requiring extended periods of coast and multiple engine restarts in a near-zero-gravity environment has brought to the forefront the important problem of coast-phase propellant management. This poses a particularly acute problem with cryogenics because of the need to vent and relieve tank pressures periodically. In turn, the problem of maintaining propellants away from vent outlets to prevent entrainment of liquid in the vent flows arises. Entrainment of liq-

[redacted]

uid in vent flows, or liquid venting, depletes available propellants for mission requirements and produces complexities in the design of true nonpropulsive and balanced vent systems.

Much work has been done to date on the behavior of cryogenic and other propellants in near-zero-gravity conditions produced for short periods in drop towers and scale-model flight tests (e.g., refs. 1 to 5). This work has produced much valuable data on fundamental laws and scaling parameters for model work. This effort, however, has not shown the interaction between forces, energies, and transients peculiar to a given configuration of operating hardware in a full-scale space vehicle.

The Atlas-Centaur vehicle AC-4 launched from Cape Kennedy on December 11, 1964, provided data giving much insight to the near-zero-gravity behavior of a cryogenic in a full-scale space vehicle. For the first time, the Centaur engines were planned to be restarted for a short duration burn.

DISCUSSION AND ANALYSIS OF FLIGHT DATA

A correlation of the post-MECO (main engine cutoff) coast-phase events are presented in the following chronological sequence:

(1) First MECO (T + 572.8 sec) to start of hydrogen venting (T + 840 sec) (where T + 0 = lift-off of vehicle)

(2) First-phase hydrogen venting (T + 840 sec) to loss of telemetry (T + 1100 sec)

(3) Acquisition of data (T + 1225 sec) to complete hydrogen venting (T + 2006 sec)

(4) Second main-engine prestart (T + 2006 sec) through retromaneuver (T + 3000 sec)

The liquid-hydrogen tank on AC-4 was extensively instrumented (see fig. 1) with skin temperature measuring devices. The majority of the following discussion, which defines the behavior and interactions of the liquid hydrogen with the vehicle, is based primarily on these temperature data and vehicle dynamics data received from downrange telemetry.

First MECO (T + 572.8 sec) to Start of Hydrogen Venting (T + 840 sec)

The vehicle at MECO was holding a flight-path angle of approximately -0.02 degree in pitch and was rolled counterclockwise approximately 15 degrees. (See fig. 2 for vehicle coordinate system and attitude engine locations.) Rates of rotation imparted to the vehicle following the MECO transient were approximately -1.0 degree per second in pitch, 0.2 degree per second in yaw, and -0.5 degree per second in roll, as shown in figure 3. Coincident with MECO, the attitude control engines were enabled to function and the propellant settling engines were ignited producing approximately 3×10^{-4} g. Attitude control engines A-2 and A-4 (shown in fig. 2) were activated immediately and burned for 1.6 seconds

to null roll rate below the threshold of the control system of 0.2 degree per second. No other attitude control engine activity was observed until T + 577.8 seconds, 5 seconds after MECO, when a programed change in the guidance steering equations commanded a pitch error of -8 degrees (command nose down) and a yaw error of -1 degree (command nose left). This maneuver was designed to give the vehicle an attitude parallel with the local horizontal and in the plane of the trajectory. Attitude control jets P-2, A-3, and A-4 responded to guidance commands immediately, and the desired attitude was achieved within 16 seconds.

Throughout the remainder of the controlled coast (to start of hydrogen venting at T + 840 sec) sporadic corrections were observed in pitch and roll, and a nearly constant duty cycle was observed in yaw (see fig. 4). Attitude control operation was more frequent than expected and was probably a result of

(1) Unpredicted propellant behavior

(2) Ullage engine exhaust impinging on main engine bells and other components in the thrust section

(3) Misalinement of the propellant settling engine thrust vector

The 30-percent duty cycle observed from the yaw rate gyro (fig. 3), is amplified in figure 5.

The disturbance accelerations, defined as the slope of the curve where the attitude control engines are off, are an indication of the distrubing torques acting on the vehicle. During the controlled coast period, the disturbance accelerations averaged 0.012 degree per second, with resulting disturbing torques of 100 to 113 inch-pounds depending on the chosen vehicle mass moment of inertia. Ullage motor misalinement to maximum design tolerances and calculated impingement forces can account for only 60 inch-pounds of torque. A center-of-gravity shift attributable to propellant location is not stable, and there were no indications of hardware movement. Therefore, motor misalinement beyond design tolerances and attitude control engine thrusts below nominal thrusts could account for the rotational rate responses observed.

Immediately on entering the coast phase, the propellant behavior was characterized by a predominantly forward movement of liquid hydrogen in the tank. Within 14 seconds following MECO, all temperature instruments on the liquid hydrogen tank surface (see fig. 6) indicated the presence of liquid hydrogen. Forward bulkhead skin temperatures and the liquid-hydrogen ullage gas temperature dropped abruptly to liquid hydrogen temperatures within 4.5 seconds, as shown in figure 7. This behavior of the liquid hydrogen can be attributed to the following disturbances as illustrated in figure 8:

(1) Fuel-boost-pump volute-bleed spray toward the forward end of the tank during boost-pump coastdown

(2) Hydrogen-duct recirculation-line spray entering the tank at station 350 on the positive x-axis during boost-pump coastdown; this spray is directed across the tank

(3) Residual slosh energy in the fluid at MECO

(4) Springback of the intermediate bulkhead and lower cylindrical section of the tank by thrust termination at MECO

(5) Backflow of mixed-phase hydrogen through the propellant ducting and boost-pump inlet at MECO, caused by a combination water-hammer effect from rapid valve closing, pressure surges from the main engine prior to engine inlet valve closing and expansion back to tank pressure and temperature of the high-energy liquid hydrogen trapped between the boost-pump and engine inlet valve

(6) Energy associated with convective thermal currents in the fluid boundary layer set up during the boost and powered phases of flight

The fuel-boost-pump volute-bleed-line flow was estimated to be initially about 340 gallons per minute. During pump coastdown, approximately 23 pounds of liquid hydrogen was returned to the tank. Similarly, the hydrogen-duct-recirculation-line return flow was estimated initially at about 40 gallons per minute maximum with 2.56 pounds of liquid hydrogen returned to the tank during pump coastdown. (See appendix A for boost-pump and flow-system descriptions.)

The possible energy inputs to the liquid hydrogen residual from these six disturbing sources have been estimated for the AC-4 flight as shown in table I.

TABLE I. - POSSIBLE ENERGY INPUTS

Source	Energy level, ft-lb
Fuel-boost-pump volute bleed	102
Hydrogen-duct-recirculation line	35
Slosh	0
Bulkhead springback	0.12
Backflow from propellant ducts	35
Energy of boundary layer due to convective currents	1.07

Further discussion and analysis of these disturbances is presented in appendix B.

The initial displacement of the liquid hydrogen in the tank by these disturbances appeared to be a wave moving forward along the positive x-axis and negative y-axis as shown in figure 6. This wetting sequence is attributed to spray from the volute bleed along the positive x-axis and spray from the recirculation line hitting the negative x-axis, dispersing laterally, and wetting the negative y-axis in the forward direction. The wave motion then continued over the forward bulkhead.

All temperature sensors indicated liquid hydrogen from MECO until approximately 50 seconds prior to venting. The propellant behavior at this time was

uncertain, but there was some evidence of drying toward the forward end of the tank, as sensors on the positive y-axis began drying from the top (fig. 6). It may be conjectured that either the propellant settling engines were beginning to settle the propellants, or some local skin drying was occurring due to heat-transfer effects.

Start of Liquid-Hydrogen Venting (T + 840 sec)

to Loss of Telemetry (T + 1100 sec)

The liquid-hydrogen vent valve was programed in the relief mode (i.e., the valve would open at or above cracking pressure) at T + 614.4 seconds. The fuel tank pressure at this time was well below the valve cracking pressure, but by T + 840 seconds it had reached the valve cracking pressure. The first indications of hydrogen venting were noted at this time. (See appendix A for vent-system description.)

The presence of liquid hydrogen at the forward end of the tank, however, resulted in mixed-phase or liquid flow through the vent system. Indicated flow rates were high, and Venturi flow temperature dropped abruptly to liquid-hydrogen levels.

Simultaneous with venting, as shown in figure 9, was the occurrence of a yaw torque input, which exceeded the capabilities of the attitude control system and produced an increasing yaw rate and vehicle spin-up.

A comparison of the predicted vehicle torques due to normal gaseous hydrogen venting with the actual measured results is shown in table II.

TABLE II. - COMPARISON OF PREDICTED VEHICLE TORQUES WITH ACTUAL MEASURED RESULTS

Condition	Vehicle torques, in.-lb		
	Pitch	Yaw	Roll
Inputs due to normal gaseous hydrogen venting	0.4	33	2
Estimated torque inputs from AC-4 flight data (maximum measured during coast)	[a]500	4500	240
Predicted control torques from attitude control system (based on center of gravity at station 343)	228	228	180

[a]Maximum torque noted at T + 915 sec was not a sustained torque.

The uncontrollable yaw torque experienced during venting was credited to large lateral impingement forces on the forward bulkhead due to venting of liquid of mixed-phase hydrogen. Lateral forces of 2 to 10 pounds in the forward bulkhead area would have produced the yaw torques noted. The predicted force

for pure gaseous venting was only 0.2 pound. Forward bulkhead skin temperatures and the liquid-hydrogen ullage temperature indicated liquid-hydrogen temperatures prior to and during venting. Thus, the theory was supported that an unknown quantity of liquid hydrogen was located in the forward end of the tank in spite of the fact that an ullage settling gravity of approximately 3×10^{-4} g had been applied to the vehicle for about 267 seconds. Also, excellent correlation of uncontrolled vehicle rates with vent periods is evident in figure 10.

By T + 905 seconds, vehicle roll had increased to 0.2 degree per second, and the yaw rate had increased to -0.5 degree per second, as shown in figure 9. At T + 915 seconds, a torquing transient in pitch and roll coupled the yaw steering error into the pitch channel causing the roll and pitch rates to reverse. By T + 1030 seconds, vehicle rates were -2.4 degrees per second in yaw, -0.6 degree per second in pitch, and about -0.5 degree per second in roll.

Hydrogen tank pressure from T + 840 to about T + 1055 seconds was unsteady but remained within the vent-valve operating range. At T + 1055 seconds, the fuel-tank pressure began a steady rise, indicating a vent flow of increasing liquid quality that was no longer of sufficient volume to relieve tank pressure. The centrifugal force due to the increased tumbling rates was settling some of the liquid hydrogen in the forward end of the tank, and pure liquid was being vented.

Acquisition of Data (T + 1225 sec) to Complete Hydrogen Venting (T + 2006 sec)

Reaquisition of data at T + 1225 seconds, as shown in figures 11 and 12, indicated that the liquid-hydrogen tank pressure, vent flow rates, and vehicle yaw rates were up sharply and increasing steadily. Figure 11 also shows a comparison of vent flow rates if pure liquid or pure gas flow is assumed. Again the inability of the tank pressure to relieve under high indicated flow rates was further evidence of liquid vent flow, which, in turn, produced an excessive yaw torque on the vehicle.

These rates continued until about T + 1366 seconds when the tank pressure, which had reached 24.2 pounds per square inch absolute, suddenly started to decrease. There was also evidence (see fig. 11) of liquid depletion at the forward end of the tank; that is, the Venturi flow rate began a decreasing trend. Ullage and Venturi gas flow temperature data, shown in figure 11, show a distinct warming and liquid-to-vapor transition in the character of the vent flow. The tank pressure decreased to the operating range of the number 1 vent valve by T + 1455 seconds.

Vehicle motion during this time, obtained from the resolver-chain output data, indicated that the vehicle was tumbling predominantly in the yaw plane with a slight nose-high attitude. The yaw rate increased from about 8.5 rpm to a maximum of about 21 rpm at T + 1550 seconds, as shown in figure 12. Pitch and roll rates during this time, as shown in figure 13 varied in a random fashion. This random nature of the pitch and roll rates is believed to be caused by the buildup and breakaway of solid hydrogen deposits at the vent exit ports. Unpub-

lished data by General Dynamics/Convair has indicated that solid deposits can build up at vent exits when a liquid or a liquid-vapor mixture is vented into a vacuum.

The dynamic response of the vehicle to apparent vent fluid quality was very pronounced. Transition from venting of liquid to venting of gas was coincident with a decreased rise in yaw rate. Significantly, however, the vent impingement forces continued to spin-up the vehicle from about T + 1450 to T + 1550 seconds (about 100 sec after the Venturi flow indicated nominal coast-phase gas flow rate). This lag was attributed to the purging of residual liquid hydrogen in the vent system downstream of the Venturi and sublimation of possible ice deposits built up on the forward bulkhead.

During the total coast-vent period, from T + 840 to T + 2006 seconds, it was estimated that 960 pounds of hydrogen were vented overboard and that about 120 pounds of liquid remained in the tank at T + 2006 seconds. Temperature sensors indicated, as shown in figure 6, that the forward end of the tank was dry; however, tank-skin temperature sensors below station 344 on the positive x-axis and the boost-pump inlet temperatures remained at liquid levels, indicating some slight residual at the bottom of the tank and in the sump.

Second Engine Prestart (T + 2006 sec) to End of Retromaneuver (T + 3000 sec)

The prestart sequence for the second Centaur main engine start (MES) began at approximately T + 2006 seconds with the vent-valve lockup and initiation of tank burp. At this time, however, as shown in figure 14, the liquid hydrogen ullage temperature dropped from approximately -380° to -420° F. Apparently, a small quantity of liquid hydrogen remained in the forward end of the tank and was entrained with the helium pressurizing gas as it blew across the forward bulkhead.

The liquid-hydrogen boost-pump start, as shown in figure 15, began at about T + 2010 seconds. Boost-pump headrise (ΔP) appeared normal (liquid being pumped) for the first 7 seconds of pump operation. Coincident with a drop in pump-inlet pressure and liquid-hydrogen ullage pressure, the pump headrise became erratic, indicating the occurrence of cavitation or vapor pullthrough. By T + 2025 seconds boost-pump headrise had peaked-out at about 25 pounds per square inch differential, and ullage pressure had dropped to approximately 14 pounds per square inch absolute. Within 5 seconds, headrise dropped to 2 pounds per square inch differential and boost-pump over-speed trip-out occurred, indicating an absence of liquid at the pump inlet.

The liquid hydrogen remaining in the tank by T + 2010 seconds had been reduced drastically as a result of liquid venting during coast. The decay of the liquid-hydrogen ullage pressure at boost-pump start can probably be attributed to the cooling of the large ullage by the liquid-hydrogen boost-pump volute bleed spray. If it is assumed that (1) all the heat required to vaporize the liquid hydrogen is extracted from the ullage gas and (2) the initial ullage tem-

perature is 60° to 65° R, then vaporizing approximately 15 to 17 pounds of the sprayed liquid hydrogen would produce the pressure drop noted. Calculations also indicated that the boost pump sprayed approximately 30 pounds of liquid hydrogen back into the tank during this time.

The command for the second MES occurred at T + 2049.7 seconds. Insufficient liquid hydrogen, as previously discussed, was available to sustain boost-pump operation and the normal engine start did not occur.

Even though the liquid hydrogen vent valve was locked up at burp, the liquid-hydrogen tank pressures remained low throughout the planned second engine burn period. At second MECO, the liquid-hydrogen tank pressure rapidly began to increase at about 2.8 pounds per square inch per minute. Heat-transfer calculations show that this pressure-rise rate would be associated with a full tank of hydrogen gas. At T + 2385 seconds, the hydrogen tank pressure reached the cracking pressure of the secondary vent valve and it relieved momentarily; 2 seconds later, the retrothrust signal was commanded, and the engine inlet valves were opened. This allowed the liquid oxygen and liquid hydrogen tanks to blow down and should have produced an axial thrust of approximately 30 pounds. Propellant tank pressures with liquid remaining in the tanks should have remained fairly steady, being sustained by boiloff gases. The absence of residual liquid hydrogen, however, resulted in the hydrogen tank pressure dropping off rather rapidly, as shown in figure 16, to 3 pounds per square inch absolute at T + 3000 seconds. Liquid oxygen tank pressure, though, remained fairly constant indicating that a quantity of liquid oxygen still remained in the tank and that the boiloff was sufficient to maintain tank pressure. Actual thrust levels produced by the engine blowdown, however, could not be assessed because the data were obscured by the vehicle spinning motion.

At the end of the engine blowdown, the engine inlet valves were closed and the tank pressure recovered gradually on subsequent orbits, being influenced by solar heating and vehicle position in and out of the Earth's shadow. The vehicle impacted in the South Pacific Ocean after completing 10 orbits.

CONCLUDING REMARKS

The Atlas-Centaur AC-4 flight revealed some problems of cryogenic propellant management associated with attempts to obtain multiple engine starts. From the flight data, the following observations were made:

1. A significant amount of kinetic energy was imparted to the propellants by the engine shutdown transients. This, in turn, caused motion of the fuel in the tank. Viscous damping was insufficient to dissipate the energy imparted to the fuel, and the propellant settling thrust was inadequate to settle the propellants.

2. The presence of liquid propellant near the vent port resulted in liquid or mixed-phase flow through the vent system. The greatly increased flow impinged on the forward bulkhead, which produced a yaw torque far beyond the recovery capability of the attitude control system, and caused the vehicle to

tumble in yaw. The formation of solids in the process of venting liquid or mixed-phase flow may have occurred, which tended to block the vent passage unevenly and further contribute to vehicle instability. The data correlation between vehicle motion and venting periods was excellent.

3. The command for the main-engine prestart sequence and second main-engine start was properly given by the programer. The fuel boost pump started on command, but operated erratically as a result of cavitation. The absence of liquid fuel in the feed lines precluded a successful second engine start.

The AC-4 flight demonstrated that forces other than molecular forces played the dominant role in determining propellant behavior even though an ullage settling force sufficient to overcome the molecular forces was provided. Most of the work to date in predicting low-gravity propellant behavior has been concentrated on molecular forces. It appears that a refocusing of attention to the effects of induced transient forces would yield greater insight and understanding in the area of propellant management.

The AC-4 flight has revealed many areas in need of attention. Among these are

1. Attenuation of transient disturbances during engine shutdown and restart

2. Evaluation of the effectiveness of energy-dissipation devices

3. Determination of the propellant settling thrust level required in relation to the magnitude of the expected disturbances

4. Development of means of gaseous venting when venting is required, in a true nonpropulsive mode to ensure vehicle stability

Studies and optimizations in these areas would be helpful in the design of future space vehicle utilizing cryogenic propellants and capable of multiple engine starts.

Lewis Research Center,
National Aeronautics and Space Administration,
Cleveland, Ohio, August 13, 1965.

[redacted]

APPENDIX A

VEHICLE AND SYSTEM DESCRIPTIONS

General Vehicle Description

The Atlas-Centaur vehicle, as shown in figure 17 is essentially a two and one-half stage vehicle whose operational purpose is to place a Surveyor spacecraft on a lunar intercept.

The first stage is an Atlas intercontinental ballistic missile whose tapered nose section has been modified to a constant 10-foot diameter. Also, eight 500-pound-thrust retrorockets have been added to the aft section to increase the rate of separation from Centaur. The tank is a fully monocoque stainless-steel structure maintaining its integrity through internal pressurization. The first stage, which weighs about 262 500 pounds at lift-off, consists of a jettisonable booster section, the sustainer and propellant-tank section, and the interstage adapter. Its propulsion system includes two booster engines, a sustainer engine, and two small vernier engines. Total lift-off thrust of the five engines is approximately 389 000 pounds, with all engines capable of gimballing for directional control.

The Centaur stage is the nation's first hydrogen-fueled space booster. The tank structure, like the Atlas, is a thin-walled 301 stainless-steel, monocoque cylindrical-section structure, pressure-stabilized to maintain its shape. The cylindrical portion is capped on each end by an elliptically shaped stainless-steel bulkhead. A double-walled ellipsoidal inner bulkhead separates the liquid oxygen and liquid hydrogen tanks. Vehicle thrust is provided by two 15 000-pound-thrust turbopump-fed regeneratively cooled engines, that use liquid oxygen and liquid hydrogen as propellants. Proper net positive suction head (NPSH) for the engine turbopumps is provided by boost pumps from each propellant tank.

AC-4 Nonpropulsive Vent System

The AC-4 nonpropulsive vent system, as shown in figure 18, consists of a standpipe, Venturi flowmeter, two vent valves, and a plenum, with opposing exits in the vehicle pitch plane. Gaseous hydrogen flow from the tank through the standpipe was measured by the calibrated Venturi. Hydrogen tank pressure was regulated by the number 1 vent valve (19.5 to 20.5 psia) during flight, with the number 2 valve (24.8 to 26.8 psia) acting only in the safety relief mode. The number 1 valve was capable of being placed in a locked or relief mode to schedule periods of vent and desired tank pressure levels. During boost, vent flow was directed through a vent stack located on the nose fairing as shown. At nose-fairing jettison, the ducting from the plenum to the vent stack and a cap on the opposing vent exit were disconnected, allowing venting in the nonpropulsive mode through the plenum exits. With gaseous hydrogen flow, torques imparted to the vehicle during vent periods were predicted at: 0.4 inch-pound in pitch, 33.0 inch-pounds in yaw, and 2.0 inch-pounds in roll.

[redacted]

Propellant Feed System

The Centaur vehicle propellant feed system is composed of three main items of hardware: propellant ducting, boost pumps, and recirculation lines. The fuel system only is described herein since the primary problem concerns the control of liquid hydrogen during the coast phase. A schematic diagram of the fuel supply system configuration on Atlas-Centaur (AC-4) is shown in figure 19. The fuel boost pump is mounted to an elbow sump on the side of the fuel tank. The main fuel supply line is a Y configuration with the common line mating with the boost-pump discharge flange, and branch lines to each engine inlet. A recirculation line attaches to each branch line just above the engine inlet to bleed off trapped gases in the ducting and thereby permit liquid at the engine inlet prior to lift-off.

The boost-pump unit consists of a centrifugal pump that is driven by a hydrogen peroxide turbine constant power (18 hp) drive. The pump specification requires a NPSH of approximately 0.1 pound per square inch to be provided to prevent cavitation. The drive has a speed limiting system that controls the turbine speed by opening and closing a valve in the peroxide feed line. In the event that the drive speed reaches a predetermined upper limit, the peroxide supply valve is automatically closed, thereby cutting off all power to the turbine. The supply valve remains closed as the turbine coasts down to a predetermined speed, at which time the valve is automatically opened again and peroxide flow is resumed. This cycling will continue indefinitely until normal operation is obtained, or until the unit is intentionally shut down by command.

The fuel pump is provided with a volute bleed line that bypasses liquid hydrogen around the impeller and permits the pump to operate without cavitation during "deadhead" operation (no flow to the main engines). This bleed flow is accomplished by slotted openings cast into the impeller housing on the discharge end. The impeller housing is enclosed by a collector manifold provided with a 1-inch outlet line that has a 13/16-inch orifice to meter the bypass flow. When the pump is installed into the elbow sump the 1-inch outlet line protrudes into a 2-inch sump-mounted bypass line that directs the bleed flow away from pump inlet and back into the hydrogen tank.

The primary purpose of the boost pump is to supply liquid hydrogen to the RL10-A3 engines with the required NPSH for all phases of engine operation. To guarantee adequate NPSH to support the engine start transient, the boost pump is started several seconds in advance of the in-flight chilldown (prestart) and MES. In the period between boost-pump start (BPS) and prestart, the engine inlet valves remain closed, and the boost pump accelerates to normal speed, where it operates in a "deadhead" mode with only the small flow through the recirculation line passing through the pump discharge. This flow has been estimated at 40 to 50 gallons per minute during the time just prior to prestart. Although the pump discharge flow is only 40 gallons per minute, an additional 340 gallons of liquid hydrogen per minute is returned to the tank by the volute bypass line during the "deadhead" period. At prestart, the main engine inlet valves and cooldown valves open allowing an additional 375 gallons per minute to flow overboard for in-flight chilldown of the main engine pumps. At MES, the cooldown valves close, the main fuel shut-off valves open and engine start occurs. For steady-state

engine operation, the boost pump delivers 1210 gallons per minute to the engines, approximately 50 gallons per minute is returned to the tank by the recirculation line, and approximately 240 gallons per minute is returned to the tank by the volute bypass line. At MECO, the engine inlet valves close, and the boost pump assumes the deadhead mode of operation. Simultaneous with MECO, the boost pump is shut down. The inertia of the rotating turbine and pump at shutdown causes the boost pump to continue rotating for several seconds (coastdown time varies, depending on whether or not liquid is retained at the pump inlet during the coast period).

The period of boost-pump operation, which is of primary interest as far as propellant behavior is concerned, is the coastdown period following MECO. During this period the pump continues to deliver liquid hydrogen back into the tank by the volute and recirculation lines at flow rates that decrease with turbine speed. This return flow contributes significantly to the disturbances in the liquid hydrogen that must be dissipated prior to venting of the tank.

Engine System

A schematic drawing of the engine system plumbing is shown in figure 20. The major components of interest are the following valves:

(1) Fuel pump inlet shutoff valve

(2) Fuel pump interstage cooldown and bleed valve

(3) Fuel pump discharge cooldown and bleed valve

(4) Main fuel shutoff valve

These valves are of primary interest because of the sequencing at engine shutdown, which is illustrated in figure 21. Note that the fuel pump inlet shutoff valve remains open after the main fuel shutoff valve is closed, which permits a short-duration high-pressure surge of hydrogen to backflow through the inlet valve and subsequently back to the tank by the fuel supply ducting and boost pump. The cooldown and bleed valves are opened before the main fuel shutoff valve is fully closed to prevent excessive pressure buildup in the system. Similarly, the inlet valve remains fully open for approximately 0.1 second after the main shutoff valve is fully closed. The inlet valve has a closing time of approximately 389 milliseconds (ref. 6).

[redacted]

APPENDIX B

CALCULATION OF ENERGY LEVELS

Fuel-Boost-Pump Volute Bleed Flow at First MECO

The flow rate as a function of time for the volute bleed flow may be calculated from the boost-pump headrise data (fig. 22) if it is assumed that the pressure drop across the bleed-line orifice is directly proportional to pump headrise. The flow equation is then

$$Q = K\sqrt{\Delta P} \text{ or } \frac{Q}{\sqrt{\Delta P}} = K \tag{B1}$$

where

Q flow rate, gal/min

K constant of proportionality

ΔP pump headrise, psi

The flow rate was determined from ground tests to be approximately 340 gallons per minute at a corresponding headrise of 28 pounds per square inch. With these known initial conditions, the flow rate for any other given headrise can be determined from

$$\frac{Q_2}{Q_1} = \frac{\sqrt{\Delta P_2}}{\sqrt{\Delta P_1}} \text{ or } Q_2 = 340\sqrt{\frac{\Delta P_2}{28}} \tag{B2}$$

where

subscript 1 initial known conditions

subscript 2 any other conditions

The instantaneous weight flow rate $\dot{w}$ (lb/sec) may be calculated from equation (B2) with the appropriate conversion factors. If a constant liquid-hydrogen density of 4.32 pounds per cubic foot is assumed,

$$\dot{w} = 0.613\sqrt{\Delta P} \tag{B3}$$

The total weight of liquid hydrogen W (pounds mass) through the volute bleed line during the post-MECO coastdown is

$$W = \int_0^t \dot{w}\, dt \tag{B4}$$

[redacted]

which represents the area under the curve shown in figure 23. The exit velocity from the 2-inch-diameter volute bleed line at any time is

$$V_e = \frac{\dot{w}}{\rho A} = 10.61\ \dot{w} \qquad \text{(B5)}$$

where

V_e exit velocity, ft/sec

$\dot{w}$ instantaneous weight flow rate, lb/sec

ρ liquid density, lb/ft^3

A exit area of line, ft^2

The incremental kinetic energy associated with a given amount of liquid pumped in a finite time period is

$$\delta KE = \frac{1}{2} \frac{\delta W}{g} V_{av}^2 \qquad \text{(ft-lb)} \qquad \text{(B6)}$$

where

δW incremental weight of fluid pumped, lb mass

V_{av} average exit velocity of fluid within finite time span of interest

Since the outlet velocity and, therefore, kinetic energy, varies over a large range during the coastdown, a numerical integration was performed by using small increments of time to calculate the total kinetic energy input to the tank.

The headrise curve of figure 22 and the formulas given in equations (B1) to (B6) were used to calculate the total liquid hydrogen returned to the tank and the kinetic energy. Results show that 22.7 pounds of liquid hydrogen were returned in the 20-second coastdown period with a total kinetic energy of 102 foot-pounds.

Fuel-Recirculation-Line Flow at First MECO

The recirculation-line-flow has been estimated between 40 and 50 gallons per minute at a corresponding headrise across the boost pump of 28 pounds per square inch differential. For the purpose of the following calculations, the lower figure of 40 gallons per minute was used. The recirculation line outside diameter as it enters the tank at station 350 is 0.625 inch with a wall thickness of 0.035 inch, which represents a flow area of 0.2415 square inch.

The same method and equations developed for the volute-bleed-flow calculations of the previous section may be utilized for the recirculation-line-flow

calculations. Changing the necessary constants results in the following equations:

$$Q_2 = 40\sqrt{\frac{\Delta P_2}{28}}$$

$$\dot{w} = 0.072\sqrt{\Delta P}$$

$$V_e = 155\,\dot{w}$$

The weight flow rate as a function of time is plotted in figure 24. Calculated results that use this data indicate a total of 2.56 pounds of liquid hydrogen returned to the tank during the 20-second coastdown period, with a total kinetic energy of 35 foot-pounds.

Backflow Through Boost-Pump Inlet

A rigorous theoretical analysis of the actual kinetic energy level of the fluid backflow into the tank is virtually impossible because of the many variables and unknowns involved. However, an estimate was obtained by utilizing films taken during low-liquid-level engine shutdowns of static tests. A camera was located at the top of the tank so that a view of the boost-pump inlet area was obtained. Films from three static tests were analyzed to establish an average velocity of the backflow wave at shutdown of 31.74 feet per second.

It was assumed that the worst condition existed in which all the liquid trapped in the fuel duct between the engine inlet valves and the boost-pump was returned to the tank. The total volume of the ducts is approximately 0.5235 cubic foot. Therefore, the mass returned to the tank is

$$\text{Mass} = \frac{(\text{Volume})(\text{Density})}{\text{Gravity}} = \frac{(0.5235\ \text{ft}^3)(4.32\ \text{lb/ft}^3)}{32.2\ \text{ft/sec}^2} = 0.0703\ \text{slug}$$

The kinetic energy associated with the mass of liquid is

$$KE = \frac{1}{2}MV^2 = \frac{1}{2}(0.0703)(31.74)^2 = 35.15\ \text{ft-lb}$$

Bulkhead Springback

The energy associated with the intermediate bulkhead springback at MECO was calculated as follows: Assume all strain energy in the bulkhead just prior to engine cutoff is transmitted into kinetic energy of the fluid. Then

$$PE = \frac{1}{2}KX^2 = KE$$

where

PE potential energy or strain energy of bulkhead

KE kinetic energy of fluid

K intermediate bulkhead spring constant, 2.06×10^6 lb/in. (calculated from ref. 7)

X deflection of intermediate bulkhead due to axial force, in.

The axial force on the bulkhead at MECO is equal to the mass of liquid hydrogen times the acceleration:

$$\text{Axial force} = F = 1084 \text{ lb mass } LH_2 \times 2.25 \text{ g's} = 2450 \text{ lb}$$

The axial force is also

$$F = KX$$

or

$$X = F/K$$

therefore,

$$PE = KE = \frac{1}{2} KX^2 = \frac{1}{2} K\left(\frac{F}{K}\right)^2 = \frac{1}{2} \frac{F^2}{K} = \frac{1}{2} \frac{(2450)^2}{2.06 \times 10^6}$$

$$= \frac{6 \times 10^6}{4.12 \times 10^6} = 1.455 \text{ in.-lb} = 0.122 \text{ ft-lb}$$

Propellant Sloshing

Although a careful analysis of rate gyro data from AC-4 revealed that propellant sloshing was insignificant prior to main engine cutoff, it should not be ignored as a potential source of disturbance. For the AC-4 configuration, the natural frequency of the liquid hydrogen would be 4.6 radians per second with a wave velocity, up the wall, as high as 2.5 feet per second for a 10-degree slosh angle.

Propellant sloshing may have been a problem during the low-thrust coast phase of AC-4. The natural frequency in the liquid hydrogen tank under 4 pounds of thrust would be 0.053 radian per second, with a period of approximately 120 seconds. Sloshing during the coast phase could not be detected because of the large number of energy inputs to the tank and the resulting disturbances (refs. 8 and 9).

Thermal Boundary Layer Energy

During ground hold and powered flight, thermal convective currents are established in the boundary layer due to environmental heating. When the vehicle acceleration is suddenly reduced at MECO, it is believed that the boundary layer would continue to move forward against a weak acceleration field. To establish the upper limit of the kinetic energy content the following equations from reference 10 were utilized. It was assumed that the boundary layer within the Centaur fuel tank would be equivalent to that of a flat plate:

$$u = U\left(\frac{y}{\delta}\right)^{1/7}\left(1 - \frac{y}{\delta}\right)^{4}$$

$$U = C_1 X^{3/7}$$

$$\delta = C_2 X^{5/7}$$

$$C_1 = 5.7826\left(\frac{g\beta q_w}{C\rho_B}\right)^{5/14}\left(\frac{Pr^{4/21}}{\nu^{1/14}}\right)\left(2.2442 + Pr^{2/3}\right)^{-5/14}$$

$$C_2 = 0.4818\left(\frac{C\rho_B \nu^3}{g\beta q_w Pr^8}\right)^{1/14}\left(2.2442 + Pr^{2/3}\right)^{1/14}$$

where

u local velocity in boundary layer, ft/sec

U equivalent free stream velocity, ft/sec

y horizontal distance from tank wall, ft

δ boundary-layer thickness, ft

X vertical distance in tank, ft

g acceleration, ft/sec^2

β volumetric coefficient of thermal expansion, $1/^{o}R$

q_w unit area heat flux at tank wall, $Btu/(ft^2)(sec)$

C specific heat, $Btu/(lb)(^{o}R)$

ρ_B fluid mass density at bulk fluid condition, lb/ft^3

[redacted]

Pr Prandtl number

ν kinematic viscosity, ft^2/sec

Figures 25 and 26 were plotted by using the preceding equations for the conditions existing in the Centaur fuel tank at MECO. The following values were used in establishing these curves:

$g = 2.25 \times 32.2 \text{ ft/sec}^2 = 72.5 \text{ ft/sec}^2$

$\beta = 0.0106/^{\circ}R$

$q_w = 0.029 \text{ Btu/(sec)(ft}^2\text{)}$

$C = 1.5 \text{ Btu/(lb)(}^{\circ}R\text{)}$

$\rho_B = 4.3 \text{ lb mass/ft}^3$

Pr = assumed unity

$\nu = 1.93 \times 10^{-6} \text{ ft}^2/\text{sec}$

Utilizing these two curves and a liquid depth at MECO of 5.5 feet results in a boundary-layer thickness of 1.9 inches at the liquid-vapor interface and a corresponding boundary-layer velocity of 0.92 feet per second. The average boundary-layer thickness is 1.34 inches. Using the average boundary-layer thickness and the maximum boundary layer velocity results in

Mass in boundary layer:

$$\text{Mass} = \frac{(\text{Density})(\text{Volume})}{\text{Gravity}}$$

$$= \frac{(4.3 \text{ lb/ft}^3)(0.112 \text{ ft})(5.5 \text{ ft})\ (31.4 \text{ ft})}{32.2}$$

$$= 2.58 \text{ slugs}$$

Kinetic energy:

$$KE = \frac{1}{2}\ (\text{Mass})(\text{Velocity})^2$$

$$= \frac{1}{2}\ (2.58)(0.92)^2$$

$$= 1.07 \text{ ft-lb}$$

[redacted]

REFERENCES

1. Petrash, Donald A.; Zappa, Robert F.; and Otto, Edward W.: Experimental Study of the Effects of Weightlessness on the Configuration of Mercury and Alcohol in Spherical Tanks. NASA TN D-1197, 1962.

2. Petrash, Donald A.; Nelson, Thomas M.; and Otto, Edward W.: Effect of Surface Energy on the Liquid-Vapor Interface Configuration During Weightlessness. NASA TN D-1582, 1963.

3. Wallner, Lewis E.; and Nakanishi, Shigeo: A Study of Liquid Hydrogen in Zero Gravity. NASA TM X-723, 1963.

4. Petrash, Donald A.; Nussle, Ralph C.; and Otto, Edward W.: Effect of Contact Angle and Tank Geometry on the Configuration of the Liquid-Vapor Interface During Weightlessness. NASA TN D-2075, 1963.

5. Knoll, Richard H.; Smolak, George R.; and Nunamaker, Robert R.: Weightlessness Experiments with Liquid Hydrogen in Aerobee Sounding Rockets; Uniform Radiant Heat Addition - Flight 1. NASA TM X-484, 1962.

6. Anon.: Design Report for RL10A-3 Rocket Engine. Rept. No. PWA FR-324C, Pratt and Whitney Aircraft, Jan. 31, 1964.

7. Pinson, Larry D.: Longitudinal Spring Constants for Liquid Propellant Tanks with Ellipsoidal Ends. NASA TN D-2220, 1964.

8. Bauer, Helmut F.: Fluid Oscillations in the Containers of a Space Vehicle and Their Influence Upon Stability. NASA TR R-187, 1964.

9. Sumner, Irving E.; Stofan, Andrew J.; and Shramo, Daniel L.: Experimental Sloshing Characteristics and a Mechanical Analogy of Liquid Sloshing in a Scale-Model Centaur Liquid Oxygen Tank. NASA TM X-999, 1964.

10. Arnett, R. W.; and Millhiser, D. R.: A Method for Analyzing Thermal Stratification and Self-Pressurization in a Fluid Container. Rept. No. 8777, NBS, Apr. 1965.

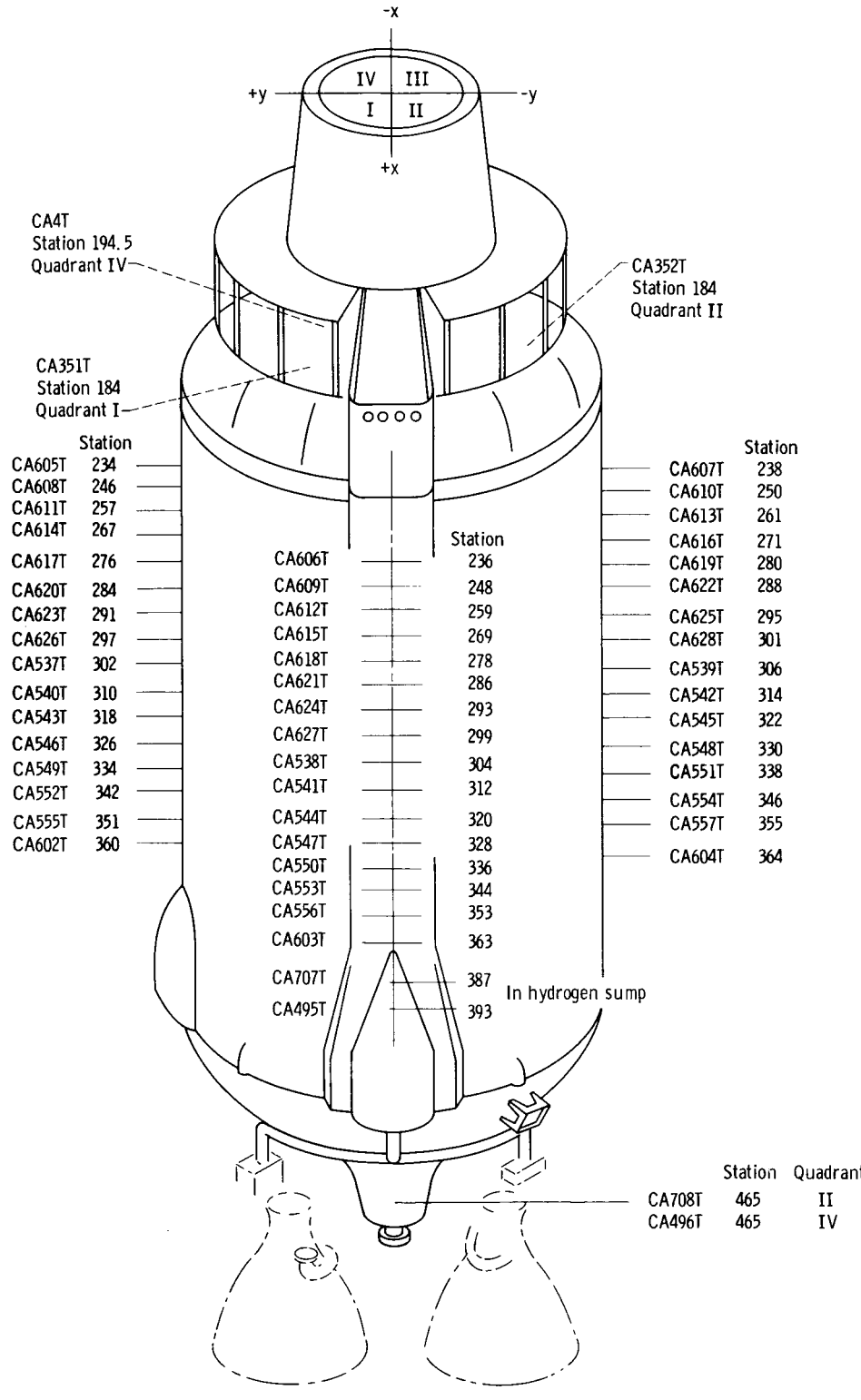

Figure 1. - AC-4 hydrogen tank external skin temperature measurements.

Engine	Thrust, lb	Function
A-1 A-2 A-3 A-4	1.5 1.5 1.5 1.5	Attitude control
P-1 P-2	3.0 3.0	Attitude control
V-1 V-2	2.0 2.0	Propellant settling

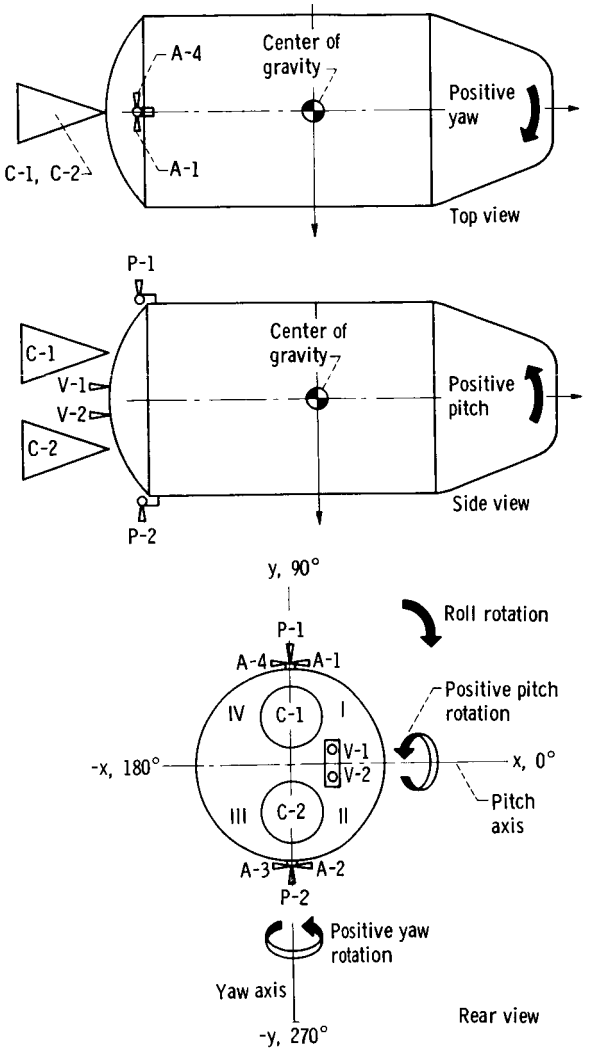

Figure 2. - Location of attitude control and propellant settling engines.

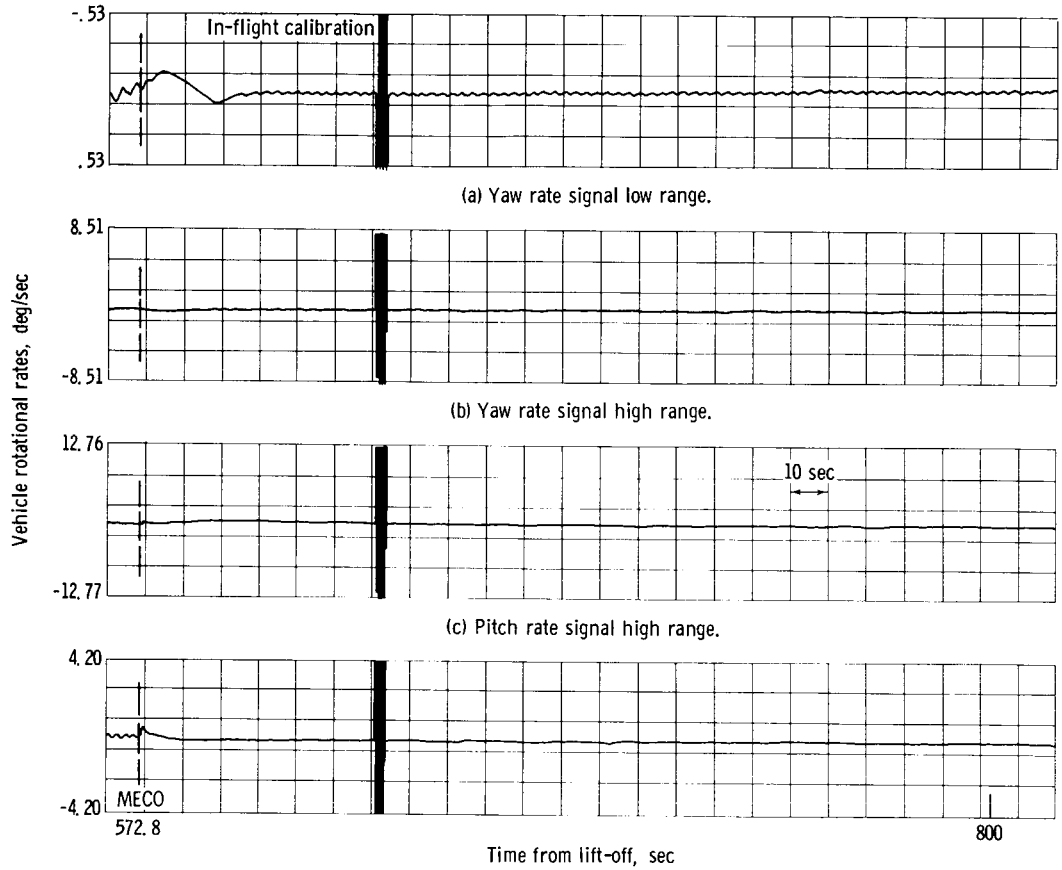

Figure 3. - AC-4 vehicle rotational rates during coast.

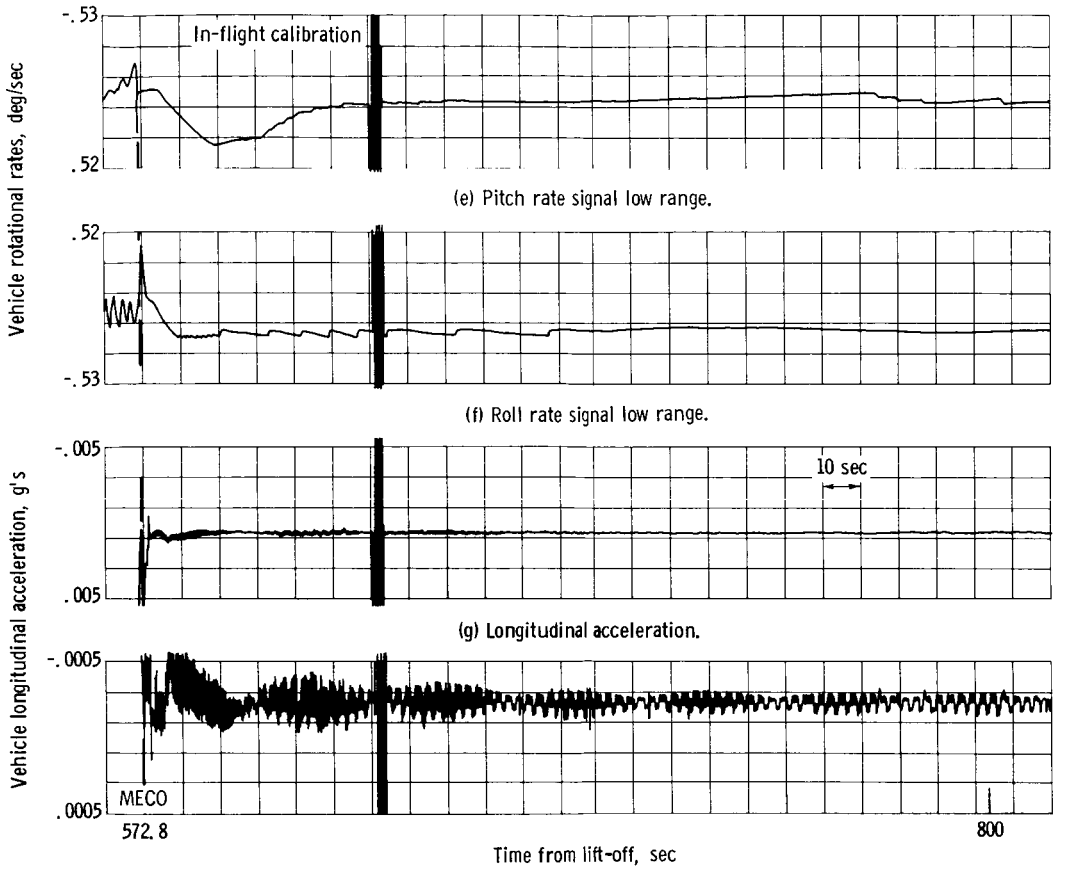

(e) Pitch rate signal low range.

(f) Roll rate signal low range.

(g) Longitudinal acceleration.

(h) Longitudinal acceleration fine range.

Figure 3. - Concluded.

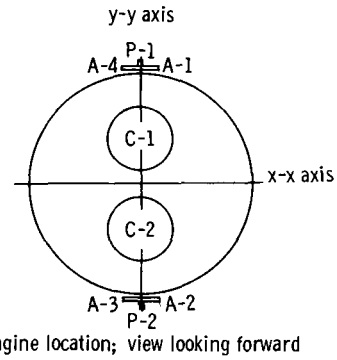

Engine location; view looking forward

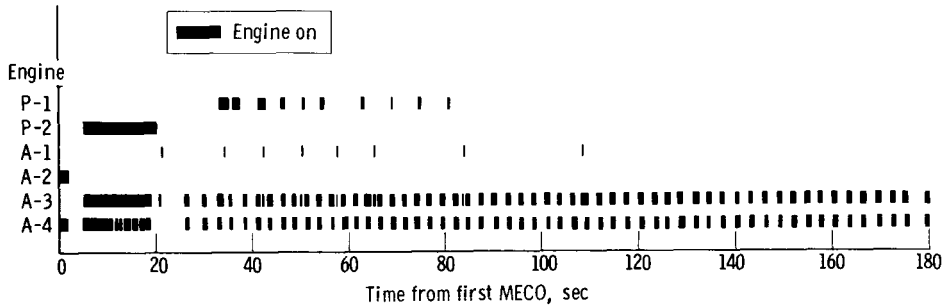

Figure 4. - Hydrogen peroxide engine commands.

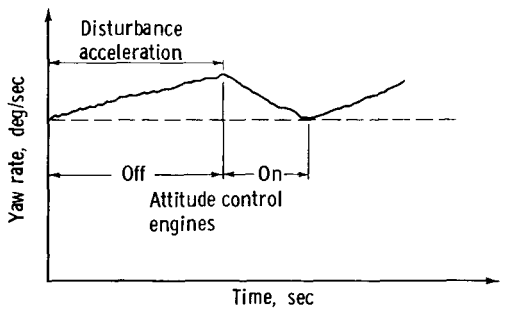

Figure 5. - Typical yaw rate gyro signal.

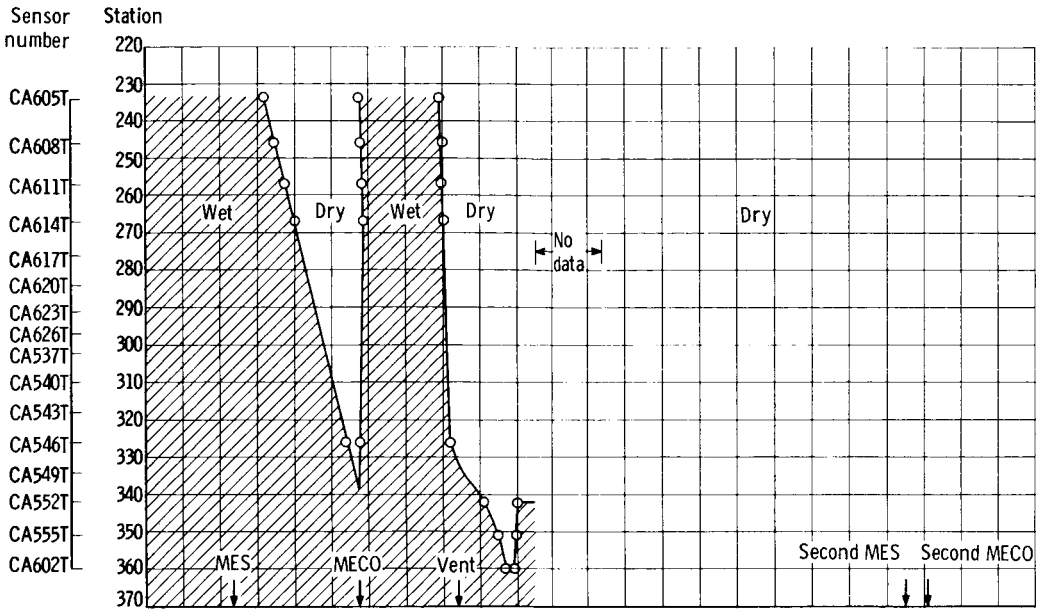

(a) Positive y-axis.

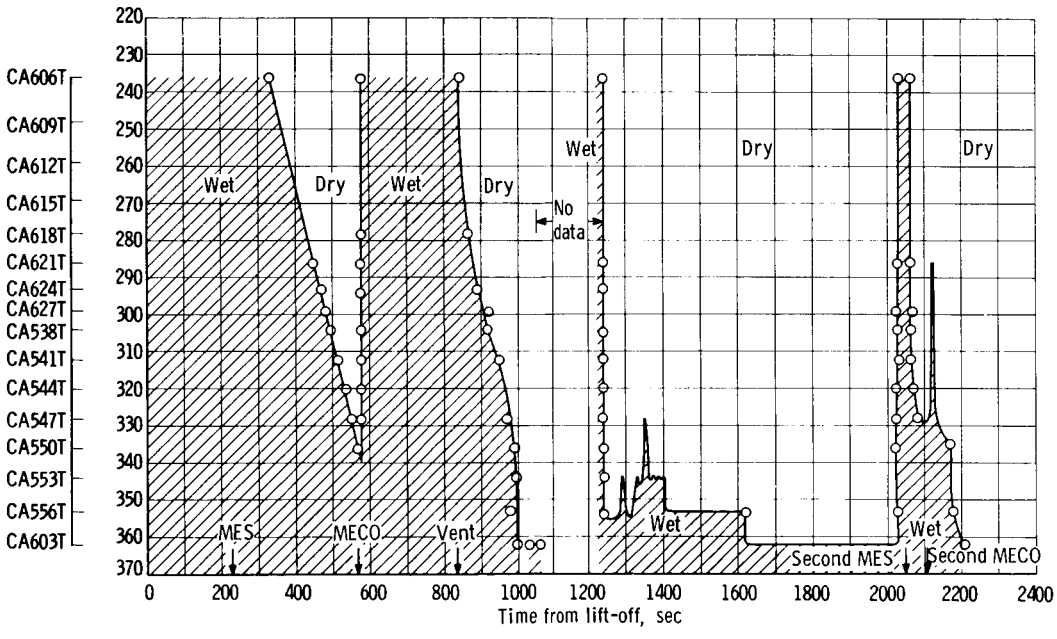

(b) Positive x-axis.

Figure 6. - Liquid-hydrogen tank wall liquid indication.

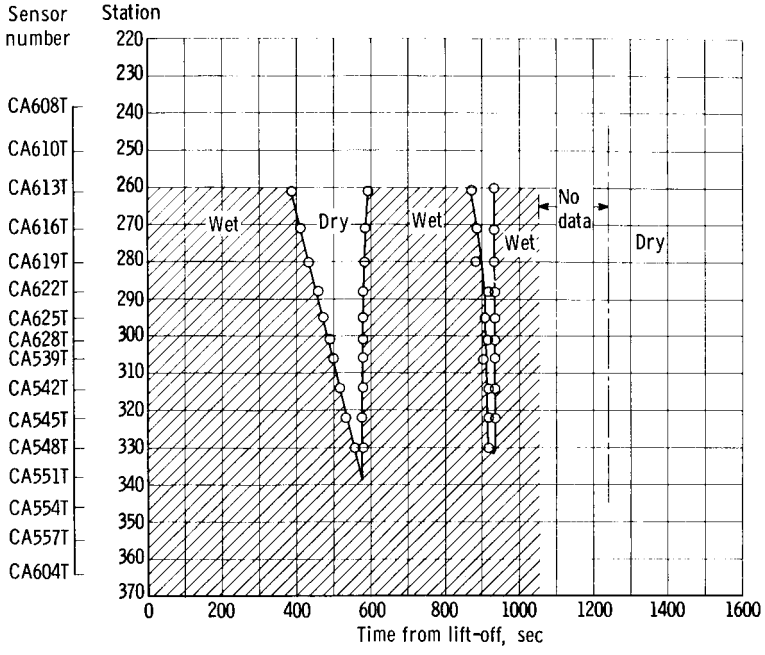

(c) Negative y-axis.

Figure 6. - Concluded.

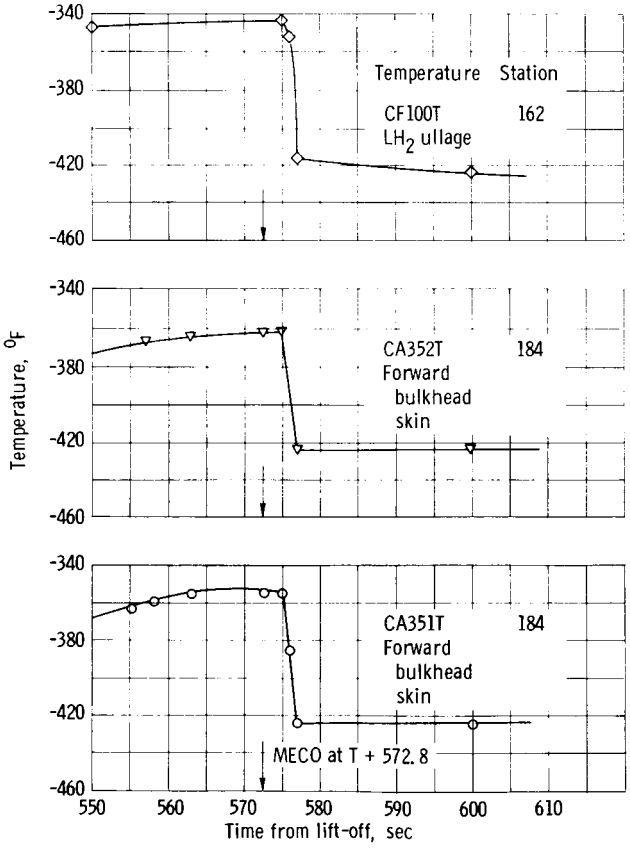

Figure 7. - Temperature history near main engine cutoff. Forward bulkhead area.

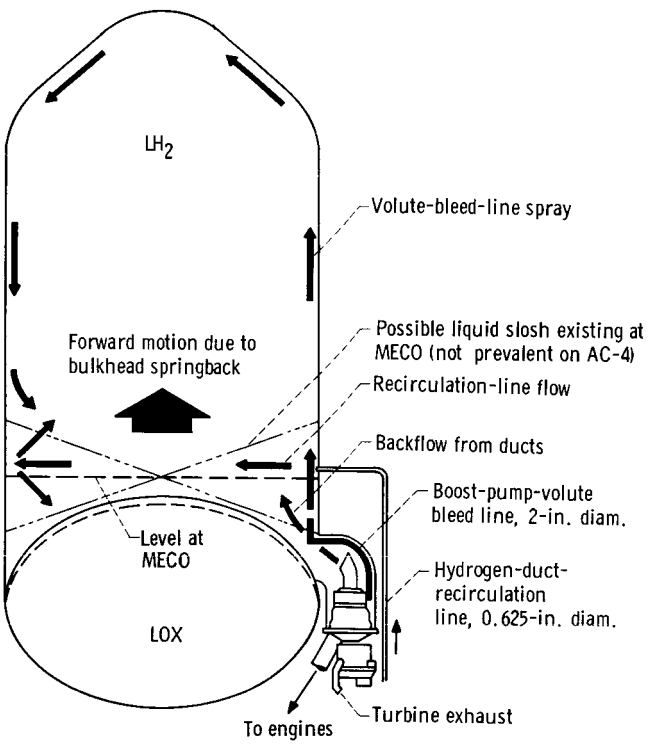

Figure 8. - Residual liquid-hydrogen motion after main engine cutoff for AC-4 flight.

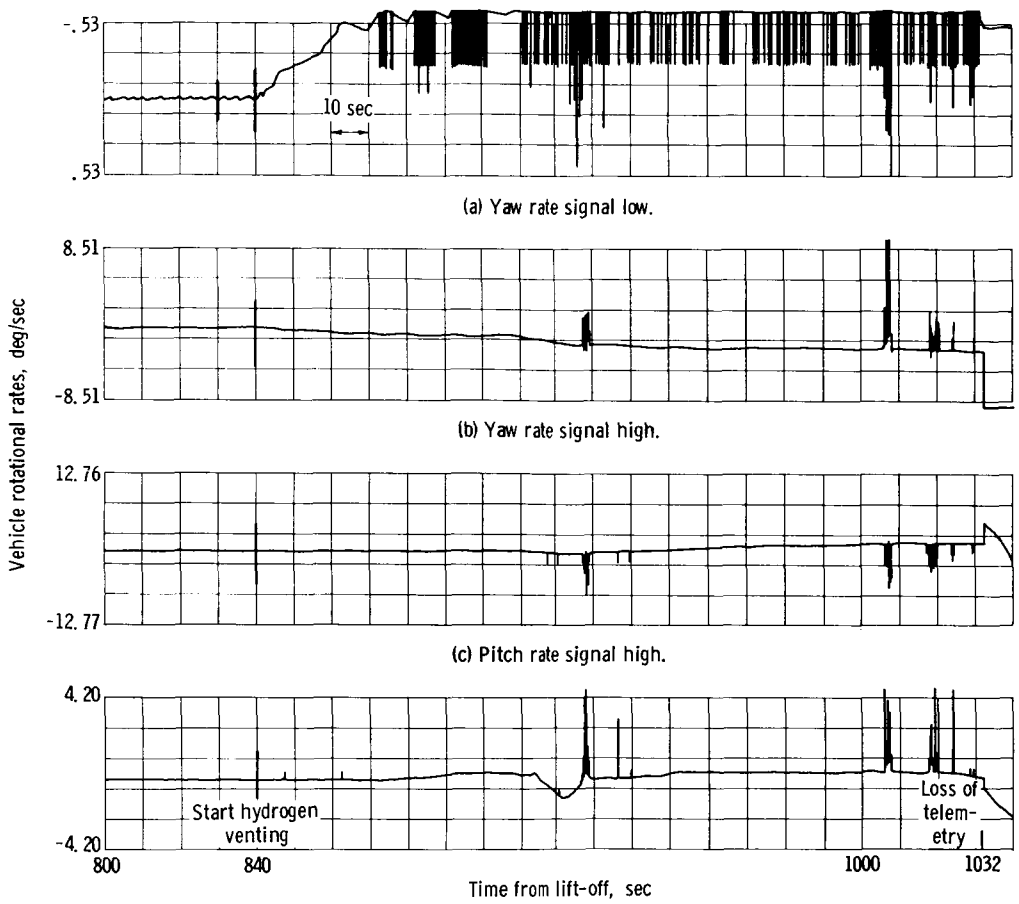

Figure 9. - AC-4 vehicle rotational rates during coast.

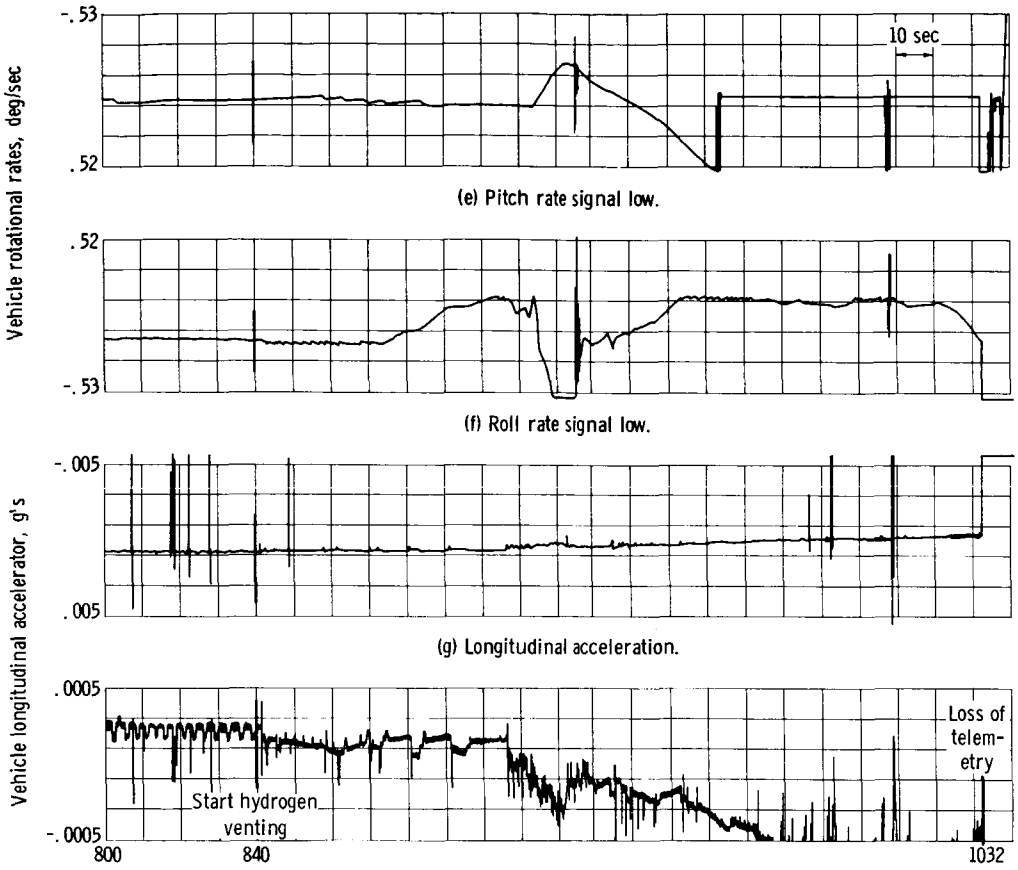

Figure 9. - Concluded.

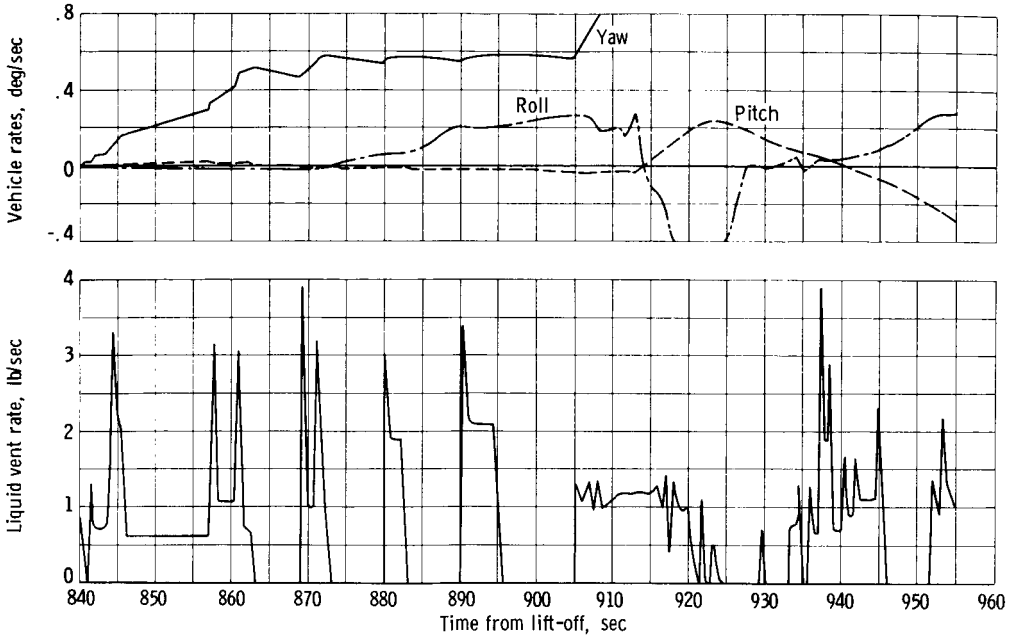

Figure 10. - Coast-phase vent and vehicle instability.

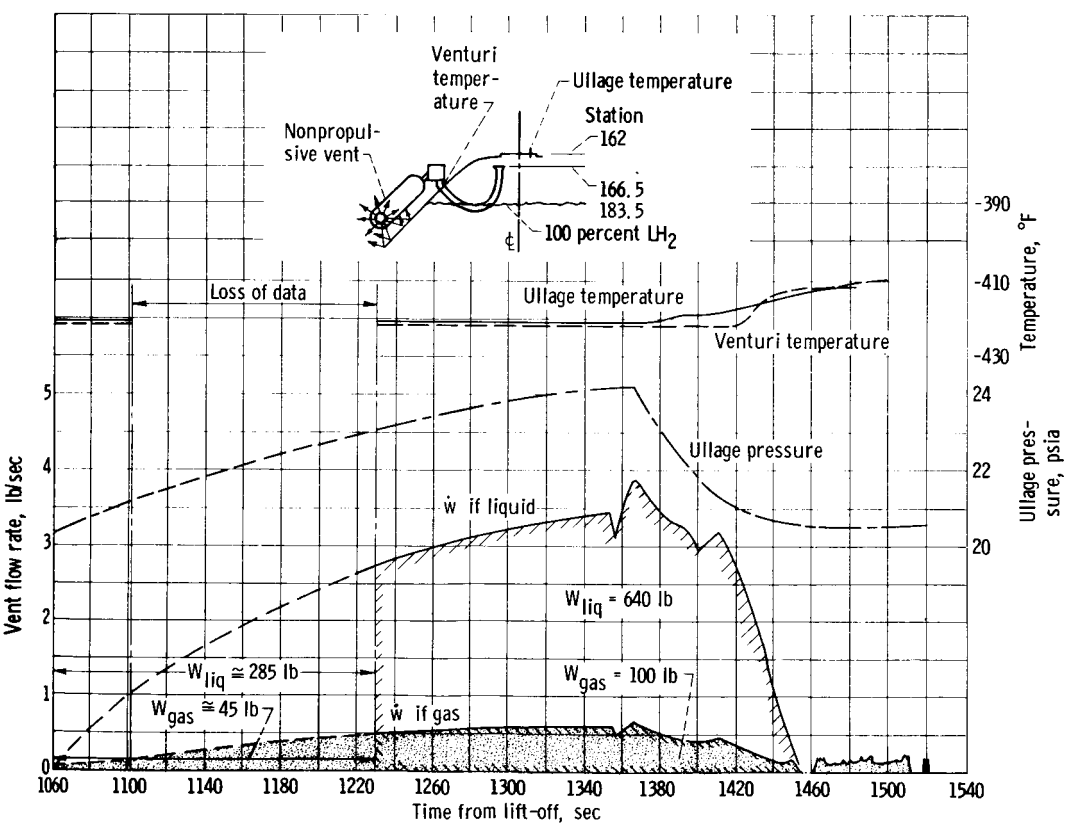

Figure 11. - Coast phase hydrogen venting.

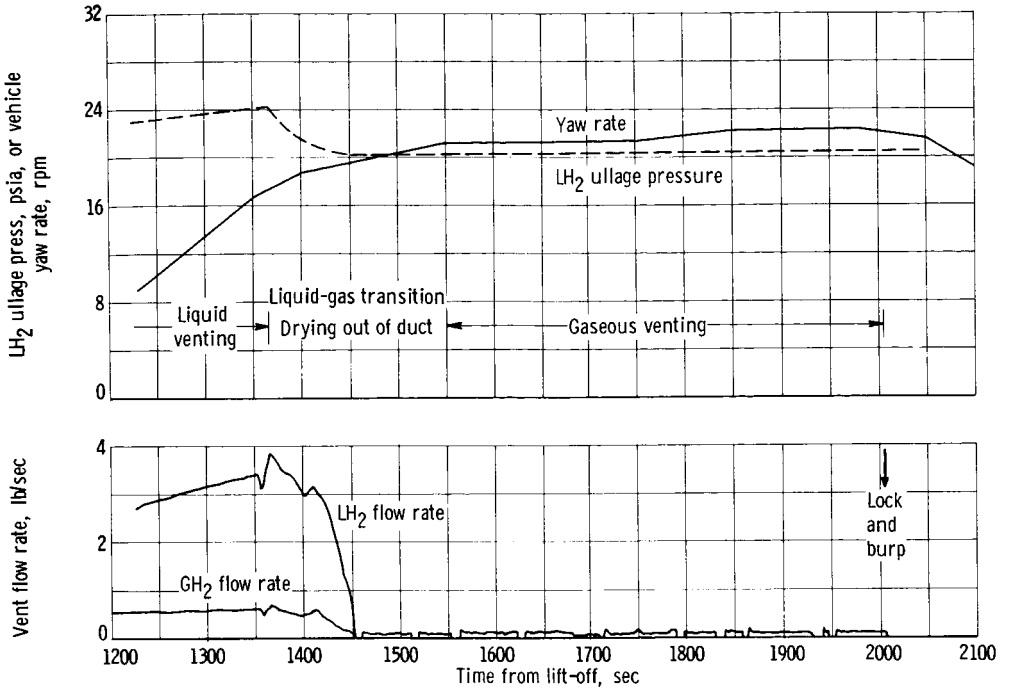

Figure 12. - Coast-phase venting and vehicle yaw rate.

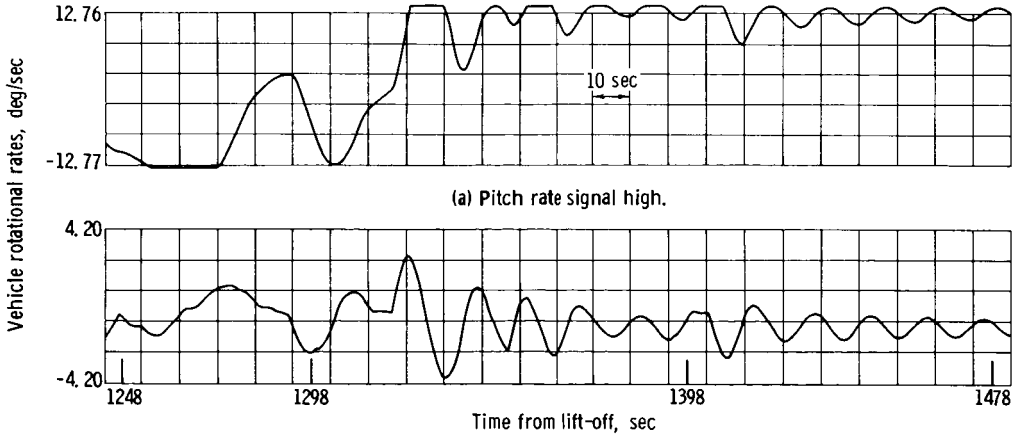

(a) Pitch rate signal high.

(b) Roll rate signal high.

Figure 13. - AC-4 vehicle rotational rates during coast.

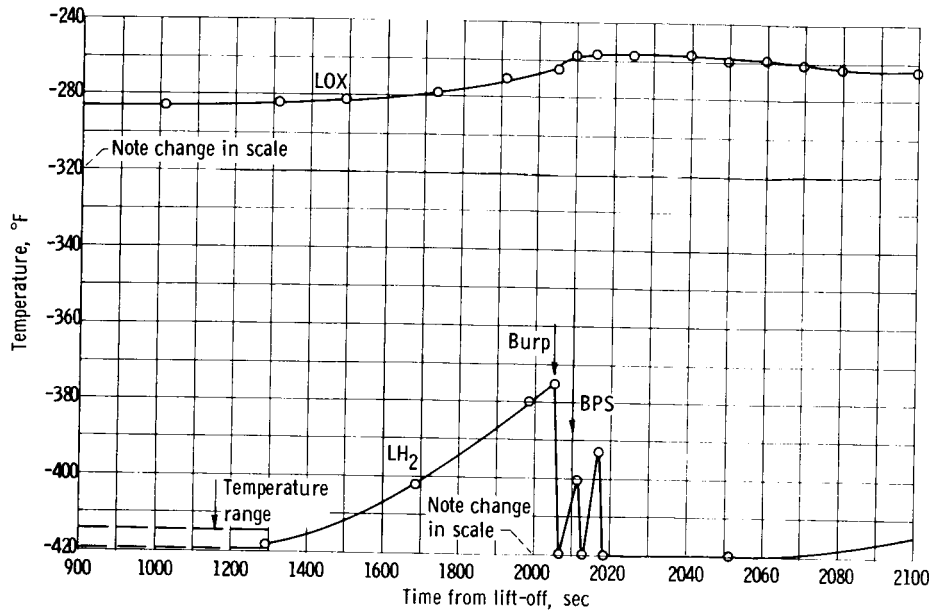

Figure 14. - AC-4 liquid-oxygen and liquid-hydrogen ullage temperatures.

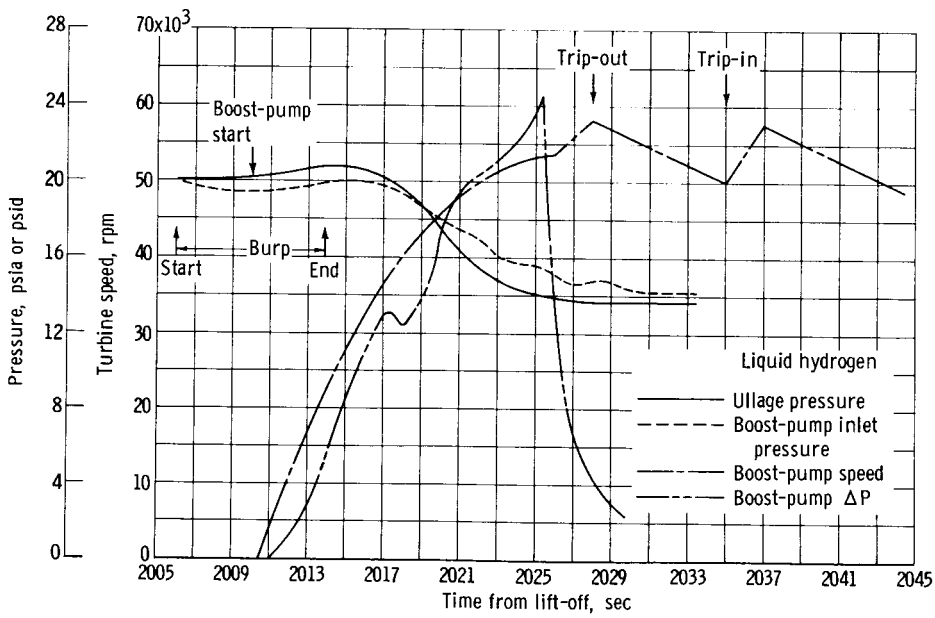

Figure 15. - Hydrogen tank pressure and boost-pump performance at second main engine start.

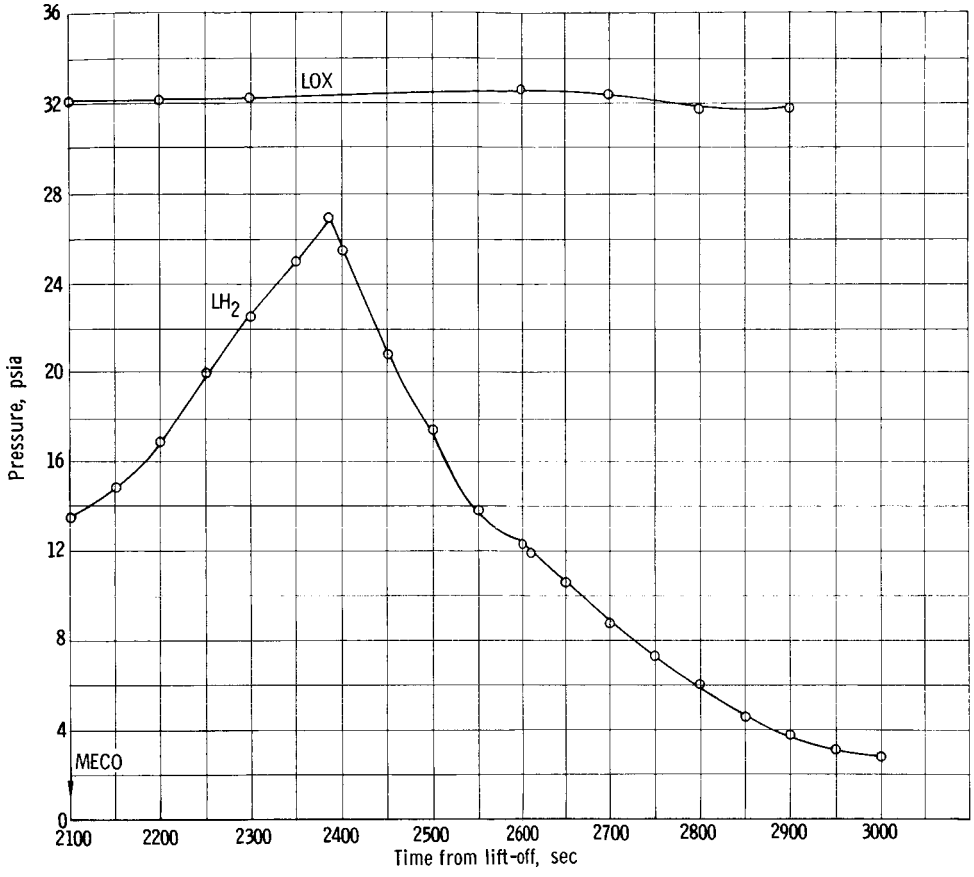

Figure 16. - AC-4 liquid-oxygen and liquid-hydrogen tank pressures.

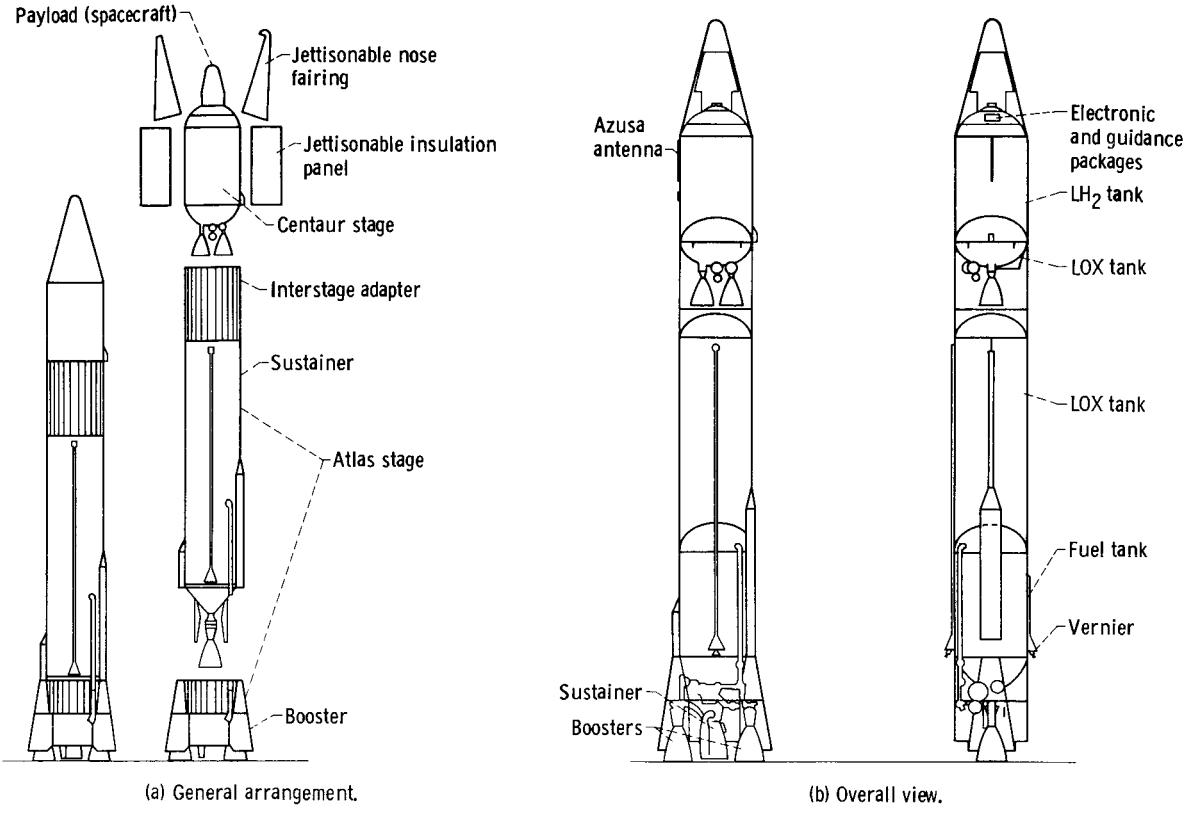

(a) General arrangement.

(b) Overall view.

Figure 17. - Atlas-Centaur vehicle.

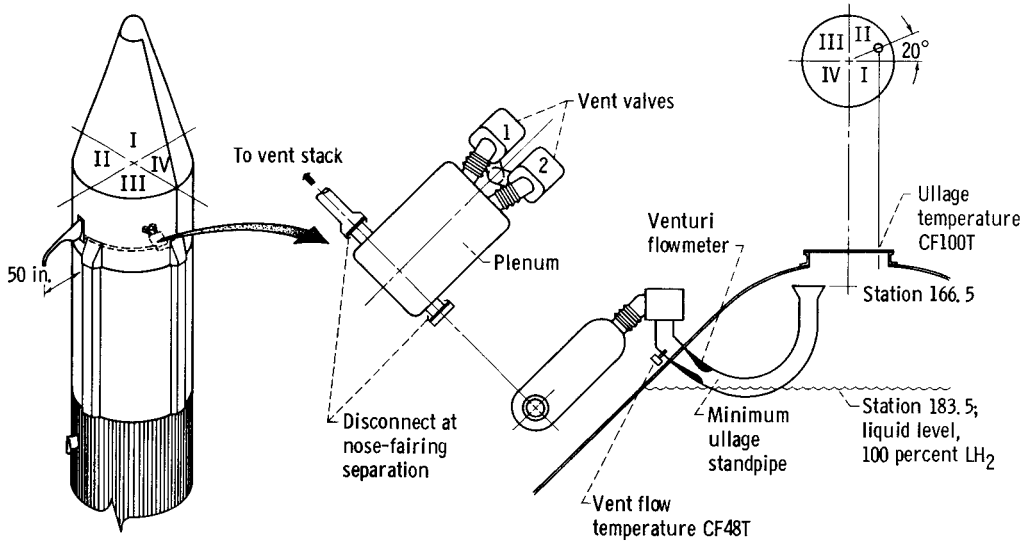

Figure 18. - AC-4 nonpropulsive vent system.

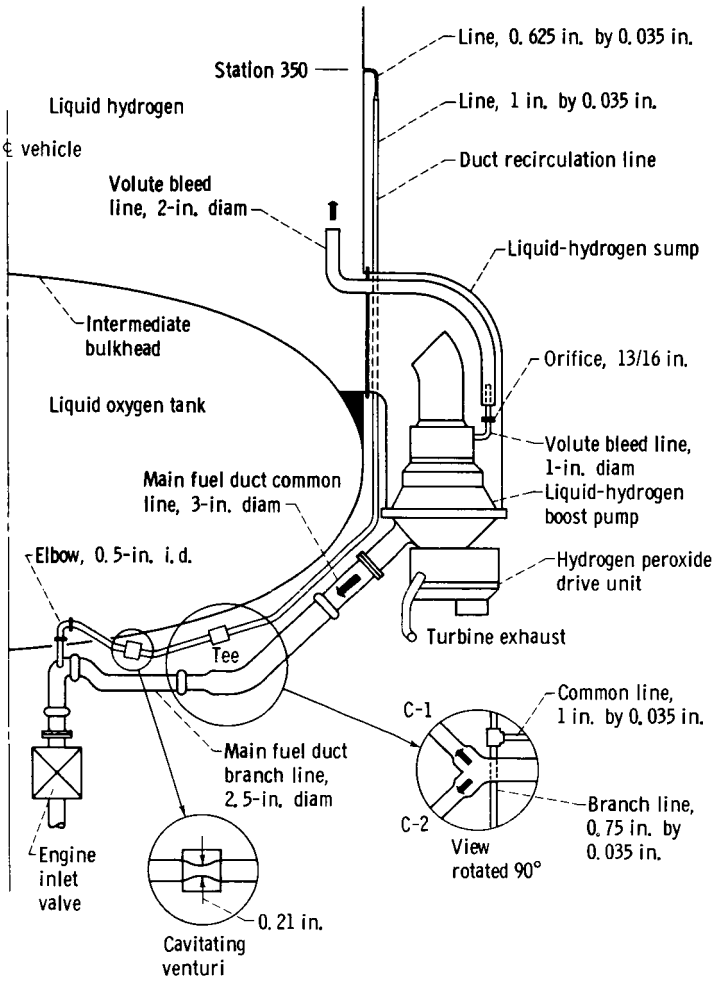

Figure 19. - Centaur liquid-hydrogen supply system.

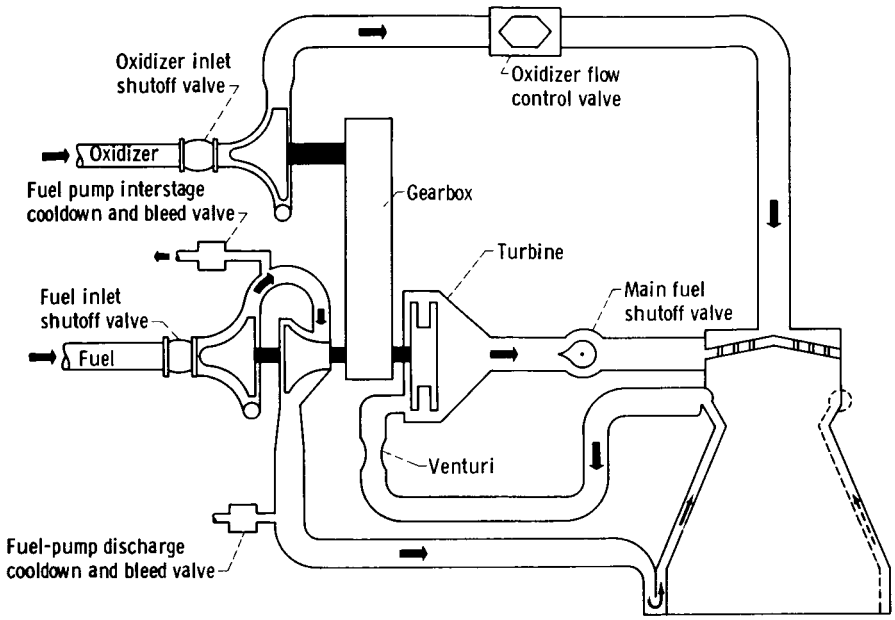

Figure 20. - RL10A-3 propellant flow schematic drawing.

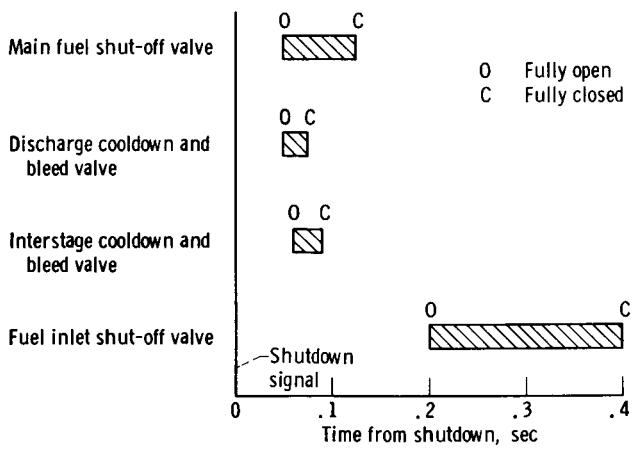

Figure 21. - Valve sequence at engine shutdown for RL10-A3 fuel system.

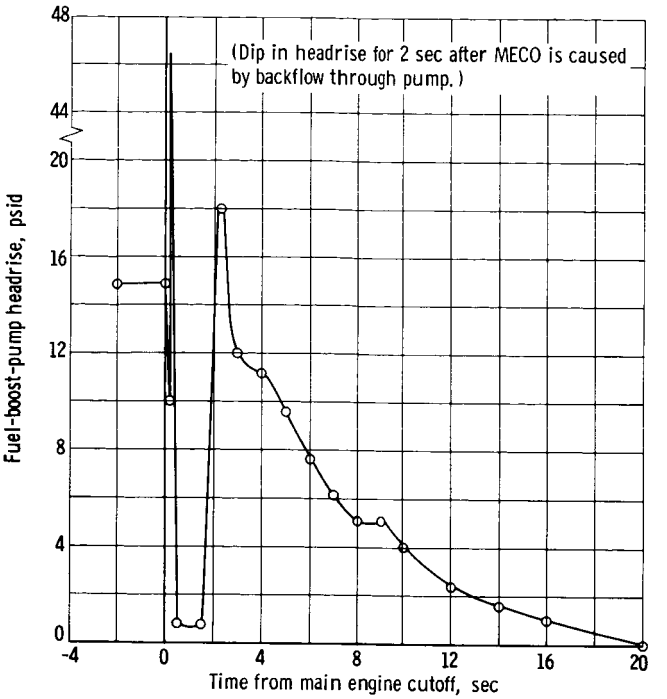

Figure 22. - Fuel-boost-pump headrise as function of time for post-main engine cutoff coastdown.

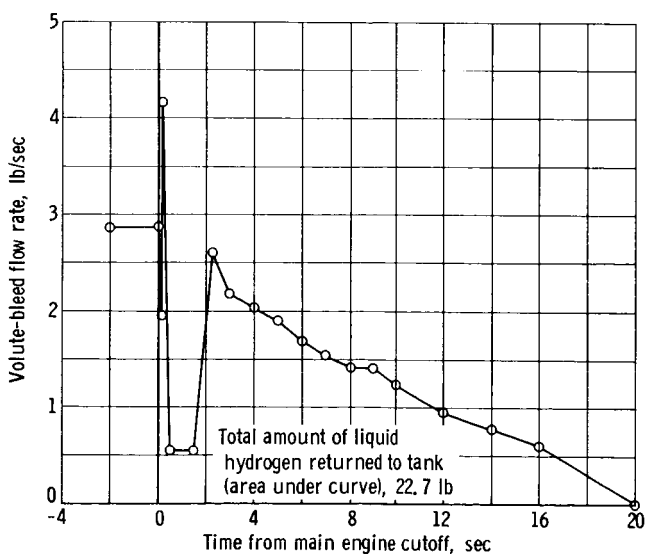

Figure 23. - Fuel-boost-pump volute-bleed flow rate as a function of time for post-main engine cutoff coastdown.

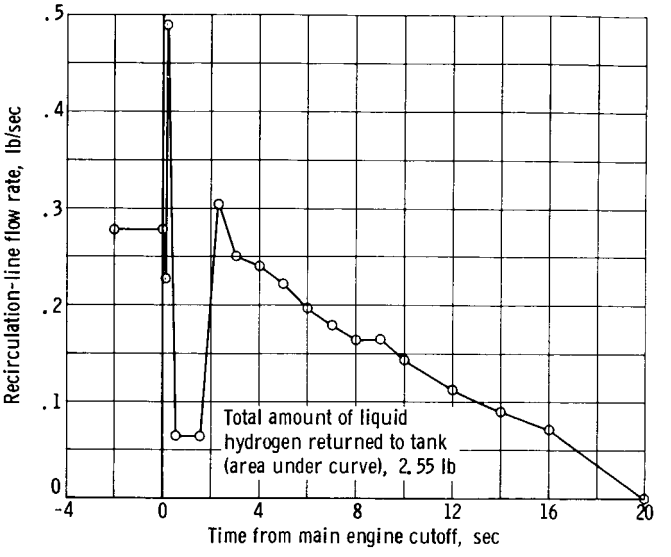

Figure 24. - Fuel-recirculation-line flow rate as function of time for post-main engine cutoff coastdown.

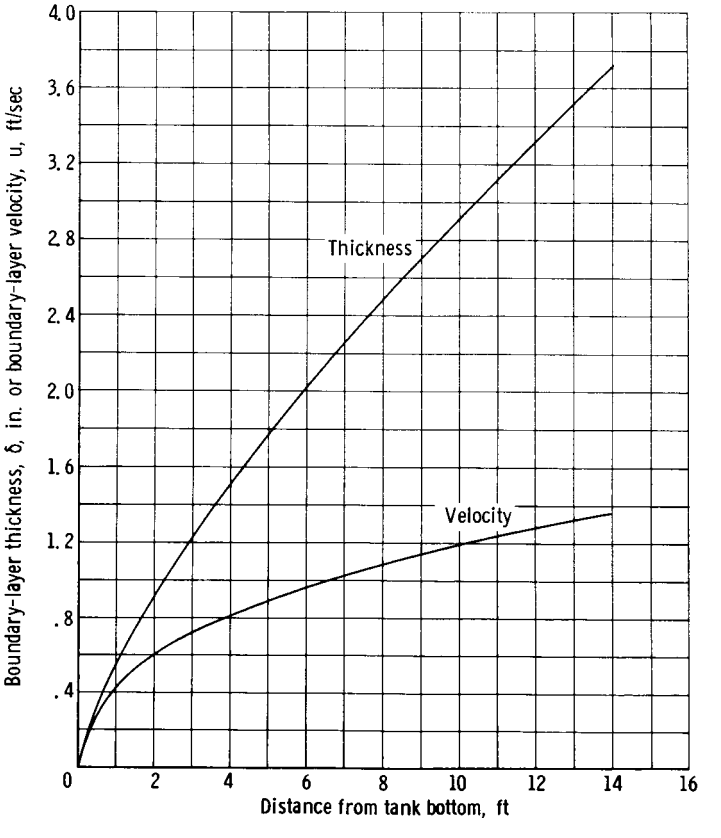

Figure 25. - Boundary-layer thickness and maximum velocity as function of distance from tank bottom.

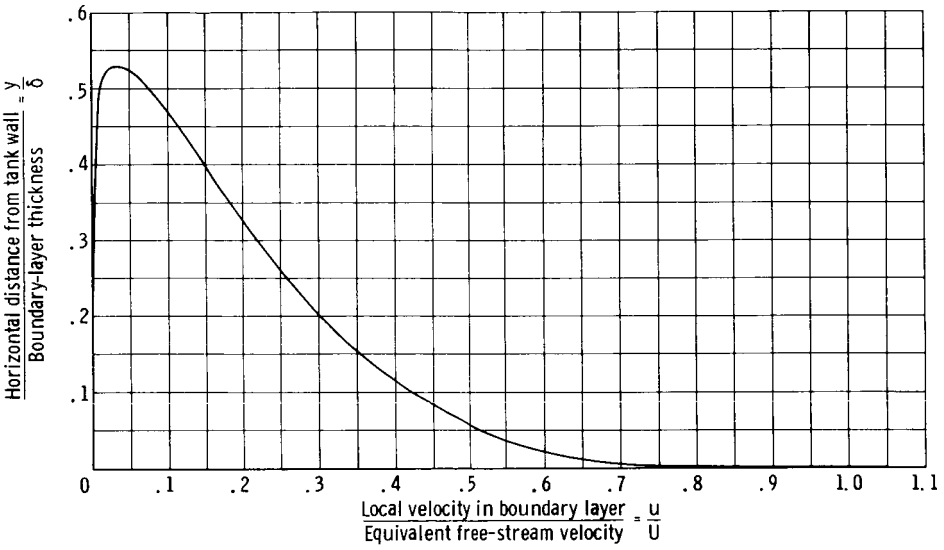

Figure 26. - Boundary-layer velocity as function of distance from tank wall.

[redacted]

"The aeronautical and space activities of the United States shall be conducted so as to contribute . . . to the expansion of human knowledge of phenomena in the atmosphere and space. The Administration shall provide for the widest practicable and appropriate dissemination of information concerning its activities and the results thereof."

—NATIONAL AERONAUTICS AND SPACE ACT OF 1958

NASA SCIENTIFIC AND TECHNICAL PUBLICATIONS

TECHNICAL REPORTS: Scientific and technical information considered important, complete, and a lasting contribution to existing knowledge.

TECHNICAL NOTES: Information less broad in scope but nevertheless of importance as a contribution to existing knowledge.

TECHNICAL MEMORANDUMS: Information receiving limited distribution because of preliminary data, security classification, or other reasons.

CONTRACTOR REPORTS: Technical information generated in connection with a NASA contract or grant and released under NASA auspices.

TECHNICAL TRANSLATIONS: Information published in a foreign language considered to merit NASA distribution in English.

TECHNICAL REPRINTS: Information derived from NASA activities and initially published in the form of journal articles.

SPECIAL PUBLICATIONS: Information derived from or of value to NASA activities but not necessarily reporting the results of individual NASA-programmed scientific efforts. Publications include conference proceedings, monographs, data compilations, handbooks, sourcebooks, and special bibliographies.

Details on the availability of these publications may be obtained from:

SCIENTIFIC AND TECHNICAL INFORMATION DIVISION

NATIONAL AERONAUTICS AND SPACE ADMINISTRATION

Washington, D.C. 20546

[redacted]